Hindawi
Advances in Civil Engineering
Volume 2021, Article ID 5783563, 15 pages
https://doi.org/10.1155/2021/5783563

Research Article

Study on the Shear Capacity of the Wet Joint of the Prefabricated Bridge Panel with a Special-Shaped Shear Key

Fan Feng, Fanglin Huang, De Zhou, Weibin Wen, and Yong Tao

School of Civil Engineering, Central South University, Changsha 410075, China

Correspondence should be addressed to De Zhou; 210026@csu.edu.cn

Received 10 May 2021; Revised 12 July 2021; Accepted 31 July 2021; Published 19 August 2021

Academic Editor: Loke Foong

Copyright © 2021 Fan Feng et al. This is an open access article distributed under the Creative Commons Attribution License, which permits unrestricted use, distribution, and reproduction in any medium, provided the original work is properly cited.

Steel-concrete composite beam has been widely applied in civil engineering, and the concrete during operation may crack due to the large shear force at the wet joint. A new concrete panel shear key with the boss is designed to strengthen the shear capacity of the wet joint part. Three different configurations of specimens are tested to study the shear capacity of the wet joint. These specimens include plain concrete specimens with shear keys, specimens with reinforcement and no shear key, and specimens with both shear keys and reinforcements. An experimental study is designed and conducted to verify the shear capacity of each specimen. The experimental results show that the ultimate shear capacity of the new wet joint structure is 73% higher than the conventional one. Meanwhile, the shear capacity of the new wet joint structure is theoretically predicted, and the finite element models are established to demonstrate the effectiveness of the experiment and the good performance of the new wet joint design.

1. Introduction

The steel-concrete composite beam is suitable for the construction of long-span bridges, such as cable-stayed bridges and x-style arch bridges. The deck system of the steel-concrete composite beam bridge is composed of steel beams and concrete panels. The bridge deck is usually prefabricated according to the size of the steel beam and installed on-site. This bridge deck system has the advantage of fast construction. However, in operation, the wet joints connecting precast bridge panels of the bridge deck system often endure shear and durability failure.

In recent years, a large number of research studies have been conducted to improve the shear capacity and durability of wet joints. These researches can be roughly categorized into three aspects: (1) improving the material performance of the wet joint, (2) improving the connecting form of reinforcement at the wet joint, and (3) optimizing the shape of the wet joint.

To improve the material performance of the wet joint, epoxy resin is adopted for the joints of the segment girder to improve the crack resistance under cyclic load [1]. At the joints of decked bulb tees and adjacent box-girder bridge, due to the action of environmental load, the two joints will bear high tensile stress. The tensile stress between the old and new concrete can be increased by using ultrahigh-performance concrete (UHPC) as the filling material of the joint [2]. UHPC is very suitable for the wet joint of the steel-concrete composite bridge [3, 4]. The ultrahigh-performance fiber-reinforced concrete (UHPFRC) joints between two precast panels reinforced with the glass-fiber-reinforced polymer (GFRP) bars can improve the mechanical performance of the wet joint [5, 6]. For the connecting form of reinforcement at the wet joint, an effective headed-bar reinforcement was designed to improve durability [7–11]. Through experiment study, Haber [12] verified the good bonding performance and crack resistance of noncontact lap splices joint combined with UHPC. As for the shape of the wet joint, the traditional construction technology of wet joint is to set a shear pocket where its surface is made of exposed aggregate finish [3]. The sawtooth, rectangular, and other special-shaped wet joints have similar mechanical properties as the traditional wet joints but have higher crack resistance [13]. Shear keys are widely used in the joints of segment bridges. Previous studies have been conducted to investigate the shear capacity of one or more shear keys

[14–17]. An internal connector in the joint of the segment bridge can reduce the negative moment of the girder [18]. A large number of research studies have also been devoted to study the mechanical properties of the shear key in an adjacent box-girder bridge by experiment or finite element methods [19–21].

To solidify the connection between the panels of the steel-concrete composite bridge, Noel et al. [22] proposed three types of shear pockets and verified the desirable shear capacity of the specimens by experiment. Zhao et al. [23] proposed a dovetail-type wet joint and studied its crack resistance under a negative bending moment. Qi et al. [7] proposed an innovative dovetail shear key that can effectively improve the crack resistance of concrete at wet joints. However, it is found that most of the present wet joints can only improve the shear capacity along a single direction vertical to the normal direction of cross section. This study is focused on a novel shear connector design to improve the shear capacity of the wet joint. The new wet joint can be used in a deck system and wet joint of an X-arch bridge as shown in Figure 1. In fact, during the operation, the wet joint is inevitably subjected to the vertical shear force and the horizontal inertia force resulted from the moving vehicle. The new shear connector of the wet joint as shown in Figure 2 is expected to have enhanced shear capacity along both the horizontal and vertical directions.

The content of this paper is organized as follows. First, in Section 2, the experiment schedule is designed to test the ultimate shear capacity of the wet joint. The experimental results are analyzed in Section 3 where the load-displacement response, strain analysis, and crack pattern are exclusively discussed. In Section 4, theoretical analysis is conducted to predict the ultimate shear capacity of the new wet joint and traditional wet joint. In Section 5, finite element analysis is provided to confirm the effectiveness of experiment analysis. Finally, some conclusions are summarized in Section 6.

2. Experimental Program

2.1. Experimental Specimens. Three different types of specimens are designed to simulate the bridge panels which are the specimens with shear keys and no reinforcement (Type 1), the specimens with reinforcements and no shear key (Type 2), and the specimens with both shear keys and reinforcements (Type 3). Each type is composed of three parts, i.e., two bridge panels and the wet joint. The bridge panels are prefabricated, and the wet joint is then cast between the two bridge panels. Figure 3 shows the assembly diagram of the experimental specimens. Figure 4(a) shows the formworks of the specimens. The formworks of the shear key are made of wood plates and steel bars. The white bars in Figure 4(a) are the PVC pipes designed to facilitate transport. Since the PVC pipes are away from the wet joint and do not affect the experiment analysis, the strain gauges are fixed on the steel bars. Figure 4(b) shows the panel-to-panel alignment. Figure 4(c) shows the fabricated experiment specimens.

The panels measure 600 mm long, 250 mm wide, and 250 mm thick. The wet joints measure 150 mm long, 250 mm wide, and 250 mm thick (see Figure 5). The experiment specimens measure 1350 mm long, 250 mm wide, and 250 mm thick (see Figure 6). The dimensions of Type1 and Type 3 with boss-type shear keys are shown in Figure 5. The cross sections of the steel bars are selected with 16 mm diameter. The overlap width of two steel bars is 80 mm.

2.2. Loading Method and Implementation. All specimens were tested with a 1000-kN servo tester. There were two supports under the specimen. As shown in Figure 7, two concentrated loads were acted on the wet joints of the specimen, and strain gauges were pasted on the specimens. The LVDT (Linear Variable Differential Transformer) and electrical-resistance strain gauges were located at the wet joint (see Figure 8). The displacement of the wet joint under the loading was measured by LVDT. Three strain gauges (CSG1-CSG3) for the concrete test were pasted on the wet joint. Four strain gauges (RSG1-RSG4) for reinforcement (i.e., steel bar) test, near the interface of the panels and the wet joint, were pasted.

2.3. Material Properties. Panels and wet joints are cast separately with the same proportion of concrete as shown in Table 1. All specimens are fabricated with the concrete of compressive strength 19.21 MPa and tensile strength 1.64 MPa. The mechanical properties of the steel bars embedded in Type 2 and Type 3 are listed in Table 2.

3. Experimental Results

3.1. Crack Pattern and Failure Mode. Figure 9 shows the crack pattern of specimens. For Type 1, when the load increases to the ultimate load, the specimen suddenly fails. The crack, through the whole specimen, appears at one of the interfaces of the panel and wet joint. After the failure, as shown in Figure 10(a), the shear key breaks.

For Type 2, when the load reaches about 50% of the ultimate load, the cracks first appear at the bottom of the wet joint. Then, the cracks in the lower part of the wet joint expand slowly, and some cracks appear in the upper part of the wet joint. When the load increases to about 73% of the ultimate load, the specimen squeaks, and interfaces of panels and wet joints appear debonding. Therein, cracks appear at the panels near the wet joint and expand with the increase of load. When the specimen is further crushed, the concrete of the wet joint moves down rapidly, and the concrete spalls locally. Figure 10(b) shows the final state of the tested Type 2.

For Type 3, when the applied load is around 45% of the ultimate load, the first crack is observed at the lower part of the wet joint. When the load increases to about 67% of the ultimate load, the specimen squeaks, but no crack propagation is observed. With the increase of load, the cracks in the wet joint increase gradually and connect with each other. When the load increases to about 80% of the ultimate load, the concrete-concrete interface appears with cracks. When the specimen is damaged, the wet joint moves down

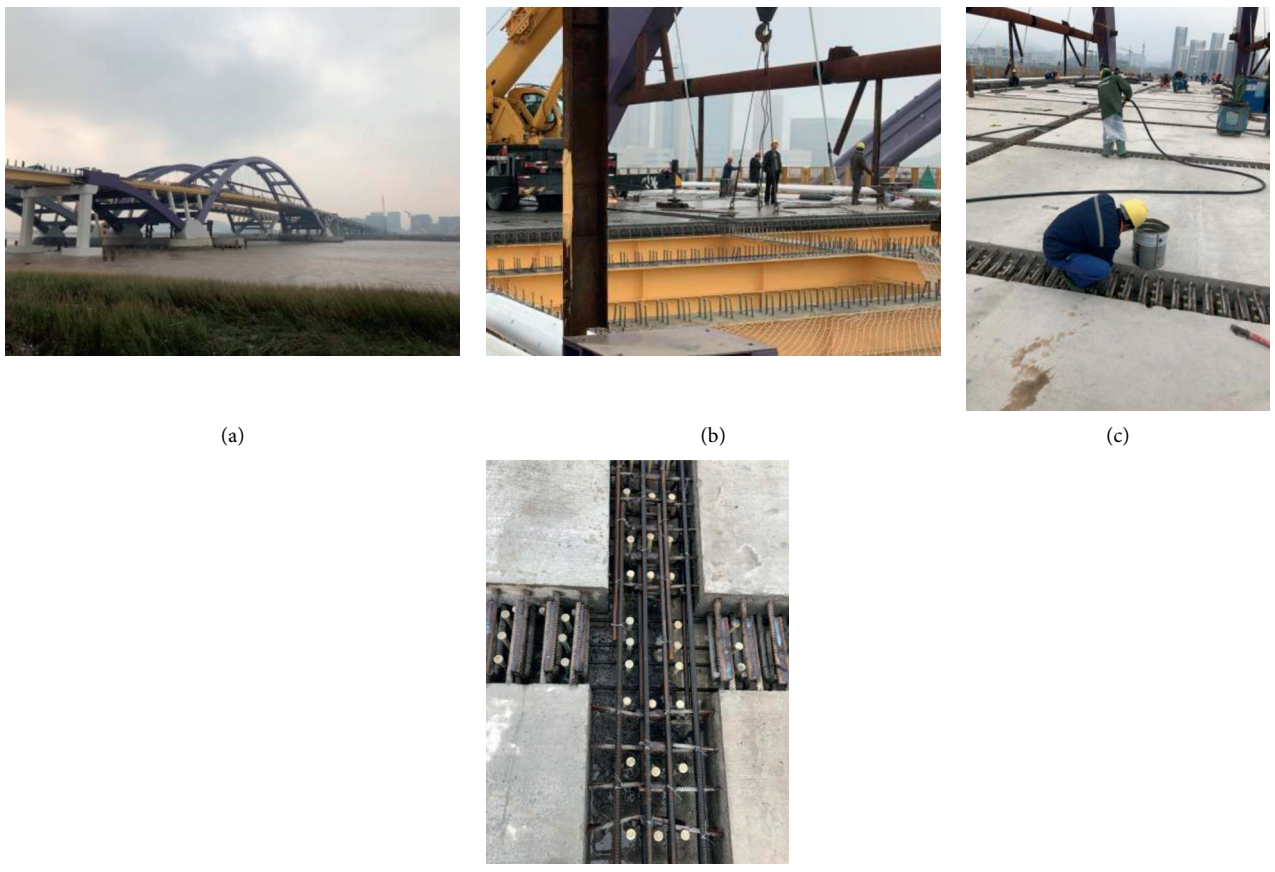

(a) (b) (c)

(d)

Figure 1: Photos of the construction site. (a) Xincheng bridge. (b) Bridge deck construction. (c) Wet joint. (d) Details of the wet joint.

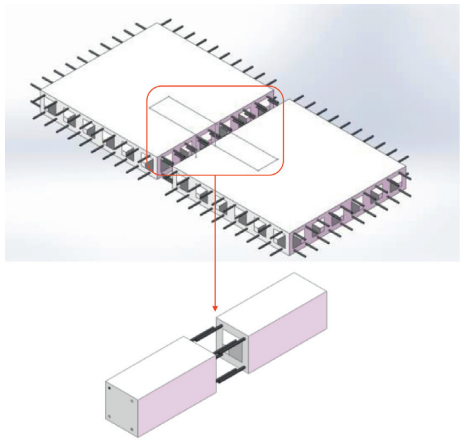

Figure 2: New type of the bridge panels and experimental specimen.

obviously, the concrete-concrete interface is staggered, and part of the concrete is separated from the main body. Figure 10(c) shows the final state of tested Type 3.

3.2. Load-Displacement Response. Figure 11 illustrates the load-displacement curves of three specimens. The ultimate shear capacity of the wet joint of the specimens can be analyzed. The curve of Type 1 changes linearly with the increase of load and decreases rapidly after the ultimate shear capacity is reached. The descending process of the curve of Type 1 is very short, which discloses the rapid fracture of the specimen.

The curve of Type 2 is linear before the load reaches 219.1 kN (about 73% of ultimate shear capacity). Then, the displacement increases rapidly. Before the displacement

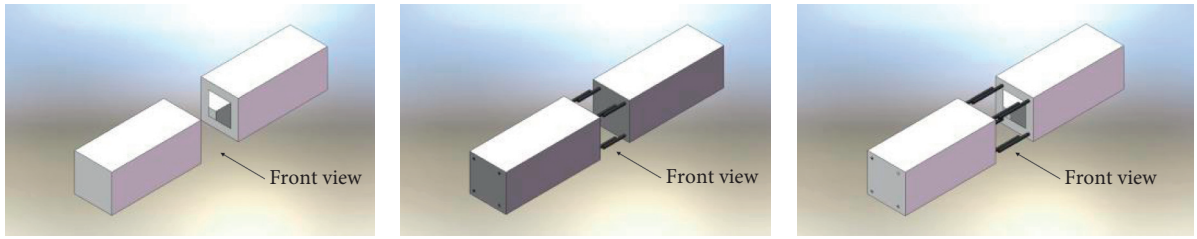

(a) (b) (c)

Figure 3: Assembly diagram of the experiment specimens. (a) Type 1. (b) Type 2. (c) Type 3.

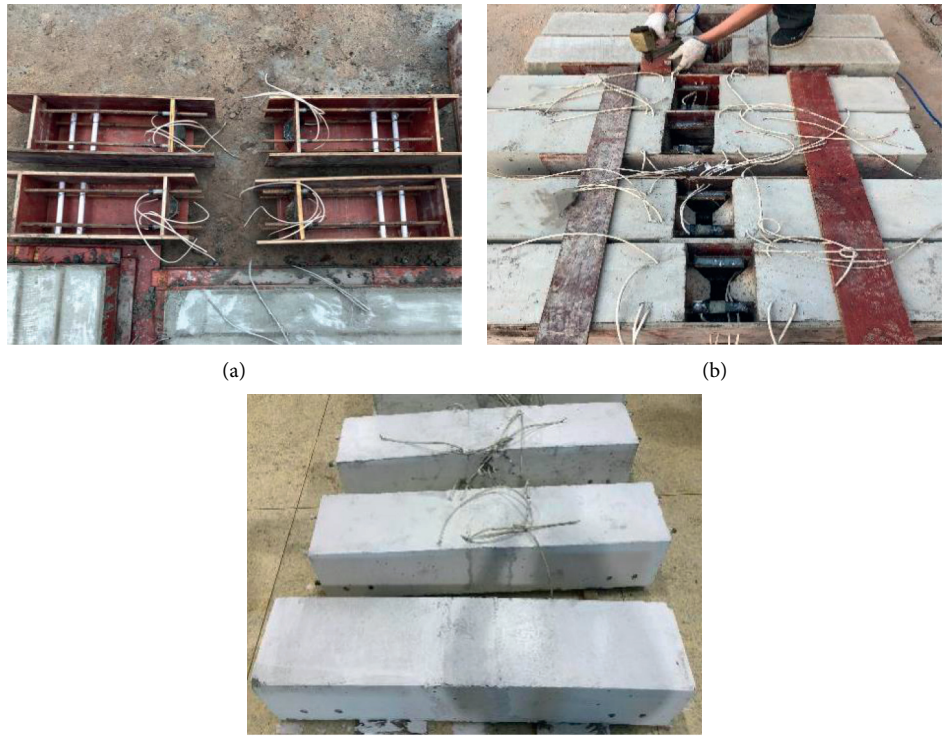

(a) (b)

(c)

Figure 4: Fabrication of experiment specimens. (a) Formworks of the specimens. (b) Panel-to-panel alignment. (c) Experiment specimens.

reaches 0.2 mm, the curve continues to rise, which is attributed to the complete debonding of the concrete-concrete interface. At this moment, the bonding force generated by the interface almost disappears, the wet joint moves down, and the steel bars begin to bear the load. When the load reaches 300.2 kN, the test is terminated when the concrete around the steel bars completely fails.

The curve of Type 3 changes linearly before the load reaches 350 kN. After that, the curve is still linear, but the slope of the load-displacement curve is clearly smaller, which may be caused by the crack propagation of the shear key. When the load reaches about 430 kN, the slope decreases drastically but remains roughly linear, which may be caused by the debonding of the concrete-concrete interface. When the load reaches 480 kN, the curve begins to change nonlinearly, which may be caused by complete shear failure and debonding of the interface. At this moment, the reinforcement bears most of the load. When the load reaches the ultimate shear capacity of 520 kN, the curve decreases gradually.

Table 3 shows the ultimate shear capacity of three types. It can be noticed that the plain concrete specimen of Type 1 has a certain shear capacity, which is about 33% of Type 2. The ultimate shear capacity of Type 3 is 73% higher than that of Type 2. Moreover, when the load for Type 2 reaches 219.1 kN, the interface has complete debonding. In Table 3, the ultimate shear strength of Type 3 improves greatly.

3.3. Strains. Figure 12 shows the load-shear strain curves of the wet joints. The value of shear strain is represented by $\gamma = 2\varepsilon_{45^\circ} - \varepsilon_{0^\circ} - \varepsilon_{90^\circ}$, where ε_{0° is the strain of CSG1, ε_{45° is the data of CSG2, ε_{90° is the data of CSG3, and γ is shear strain.

The shear strain of the specimens is compressive strain, so the value varies in the negative region. With the increase of load, the shear strain of Type 1 increases. The curve is

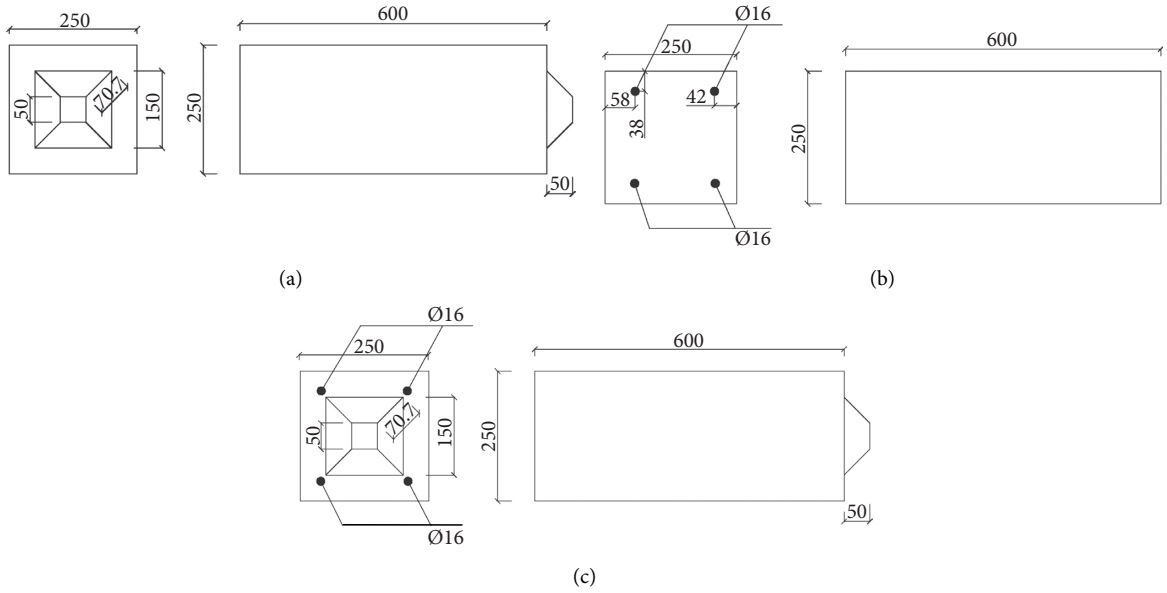

Figure 5: Dimension of the panels. (a) Dimension of Type 1. (b) Dimension of Type 2. (c) Dimension of Type 3.

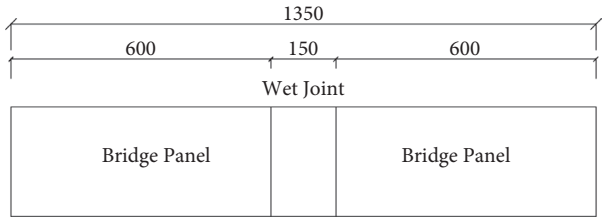

Figure 6: Dimension of the experiment specimens.

roughly linear before the load reaches 60 kN and then nonlinear until the specimen is damaged. The shear strain of Type 1 increases greatly and approaches 3000 at failure. The curve slope of Type 2 changes when the load reaches 160 kN and changes again when it reaches 220 kN. This is the time when interfacial debonding occurs. The slope of the curve is gradually decreasing. The curve ends at 240 kN. This is due to the occurrence of cracks near the strain gauge, resulting in data interruption. The curve slope of Type 3 first changes when the load reaches 165 kN and then changes again at 240 kN. When the load reaches 350 kN, the curve has a sudden change. This is similar to the load-displacement curve. Then, the slope do not change until the specimen is destroyed.

Figure 13 shows the load-strain curve of reinforcements. The curves of Type 2 lower reinforcements, measured by RSG 2 and RSG 4, change when the load reaches 180 kN. The curves of the upper reinforcements, measured by RSG 2 and RSG 4, change when the load reaches 220 kN. At this time, it is time for the concrete-concrete interface debonding. It can be judged that the interfacial debonding develops from bottom to top. The curves of Type 3 change greatly when the load reaches 350 kN. At this time, although no debonding phenomenon is observed at the interface of the specimen, the reinforcement begin to bear the load.

4. Prediction of the Shear Capacity

To predict the ultimate shear capacity of three types of wet joints, a theoretical analysis is provided in this section.

Figure 14(a) shows the detailed configuration of Type 2, and l, h, and A_1 are length, height, and area of the section, respectively. Figures 14(b)–14(d) illustrate the detailed dimensions of Type 1 and Type 3. In the figures, l_1, l_2, l_3, h_1, h_2, h_3, α, A_2, A_3, and A_4 define the geometry of three specimens.

A_1, A_2, A_3, and A_4 can be calculated by the following formulas:

$$\begin{aligned} A_1 &= l \cdot h, \\ A_2 &= 0.5 \cdot (l_1 + l_2) \cdot l_3, \\ A_3 &= l \cdot h - l_2 \cdot h_2 + l_1 \cdot h_1, \\ A_4 &= 3A_2. \end{aligned} \tag{1}$$

Assume that the ultimate shear capacity of the wet joint with no shear key and reinforcement is F_1 (see Figure 15(a)). There are a pair of cohesive forces of value F_C between the wet joint and panels. The joint is about to slip when it is up to the ultimate shear capacity, and at this state, F_1 is equal to F_C. The cohesive stress of wet joints and panels is denoted by σ_C and can be calculated by $\sigma_C = c_d \cdot f_{ct\,d}$.

The cohesive stress of wet joints and panels is denoted by σ_C which is determined by $\sigma_C = c_d \cdot f_{ct\,d}$ [24–26], where c_d is cohesion coefficient and is selected as $c_d = 0.492$. $f_{ct\,d}$ is the tensile strength of concrete. Then, F_C can be easily obtained as $F_C = 2A_1\sigma_C$

As shown in Figure 15(b), the failure of Type 1 can be considered as the shear and sliding failure of interfaces of the wet joint and panels. Shear stress $\tau_{\max}$, on the area A_2 as shown in Figure 14(b), is obtained by the maximum shear stress theory as $\tau_{\max} = \sigma_1 - \sigma_3/2 = 3F_t/2lh \le [\tau]$, where $\tau_{\max}$ is the ultimate shear stress of concrete, $[\tau]$ is calculated by

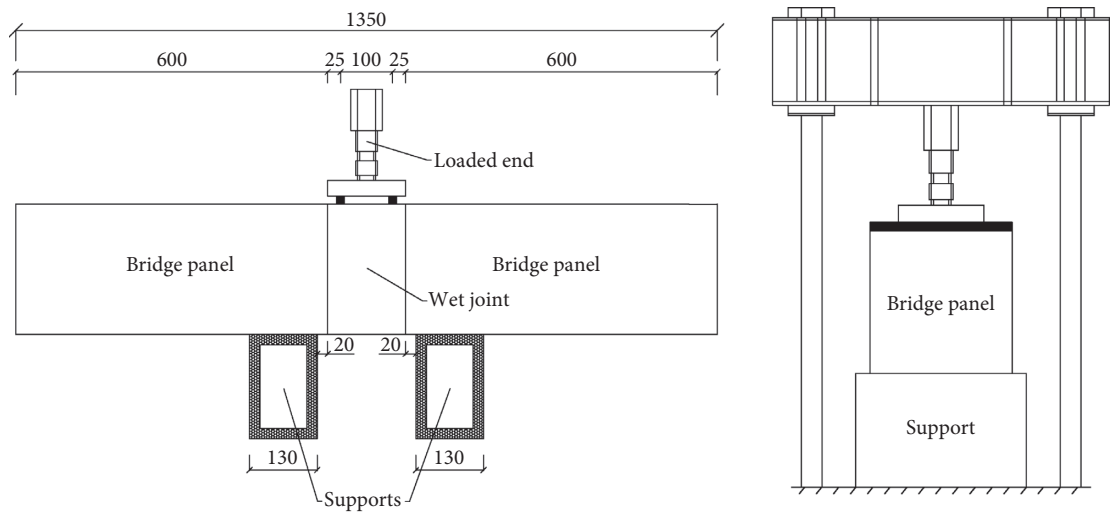

Figure 7: Loading process.

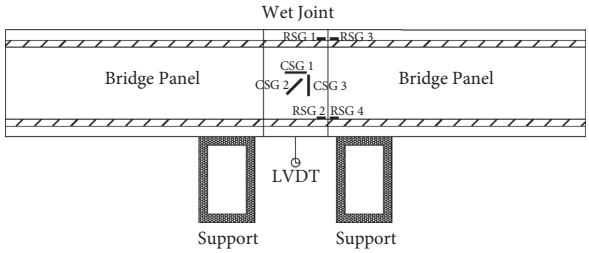

Figure 8: Sensors setting.

Table 1: Mix proportion of concrete for specimens.

Cement (kg/m^3)	Stone (kg/m^3)	Sand (kg/m^3)	Water (kg/m^3)
450	1092	735	118

Table 2: Mechanical properties of the reinforcements.

d_r (mm)	Grade	E_f (GPa)	f_y (MPa)	f_u (MPa)
16	HRB400	202	424	601

Note. d_r is the diameter for steel bars; E_f is the modulus of elasticity; f_y is the yield stress; f_u is the ultimate stress.

the formula $[\tau] = 0.3\sqrt{f_c}$, and f_c is the shear strength of concrete [27]. σ_1 and σ_3 are the principal stresses. In Figure 15(b), F_t is the reaction load acted on the area A_2. The force balance equation for Type 1 is obtained as

$$F_2 = F_t + F_C, \tag{2}$$

where F_2 is the ultimate shear capacity at the joint of Type 1, and a pair of cohesive forces F_C are acted on A_3 and A_4. For Type 2 in Figure 15(c), as the shear force increases, the concrete first slides along the interfaces of the wet joint. Furthermore, when the cohesive stress attains its maximum, the concrete bonded with reinforcements is gradually crushed. At this state, the force on reinforcements, briefly denoted by F_R, can be calculated by the following formula:

$$\begin{aligned} F_R &= \int_0^{\pi} R\mathrm{d}\theta \cdot L \cdot \sin\theta \cdot f_{ck} \\ &= f_{ck} \cdot 2RL = f_{ck} \cdot A_R, \end{aligned} \tag{3}$$

where f_{ck} is the ultimate compressive strength of concrete. A_R is the equivalent compression area of the reinforcement. R is the radius of the cross section of the reinforcements. L is the length of the wet joint. The angle θ is illustrated in Figure 16.

As shown in Figure 15(c), the ultimate shear capacity of Type 2 is F_3. F_R' is the reaction force of the F_R. With force balance of the wet joint, F_3 can be calculated by

$$F_3 = F_C + 4F_R'. \tag{4}$$

In Figure 15(d), F_4, the ultimate shear capacity of the wet joint of Type 3, can be calculated by

$$F_4 = F_C + F_t + 4F_R'. \tag{5}$$

Then, the ultimate shear capacity F of the specimen with reinforcement can be expressed as

$$F = F_C + \mathrm{sign}(\sin\alpha) \cdot F_t + F_R', \tag{6}$$

where $\mathrm{sign}(\sin\alpha)$ satisfies the following conditions:

$$\begin{cases} \alpha = 0, & \mathrm{sign}(\sin\alpha) = 0, \\ \alpha > 0, & \mathrm{sign}(\sin\alpha) = 1. \end{cases} \tag{7}$$

5. Numerical Analysis

In this section, the finite element analysis (FEA) is conducted to confirm the shear capability of three types of wet joints. A three-dimensional nonlinear finite element model is established, and the feasibility of FEA is verified by comparing the numerical results with the experimental results.

The material parameters for the numerical model are provided in Section 2.3. In this study, the mechanical behavior of concrete is modeled using the concrete damaged

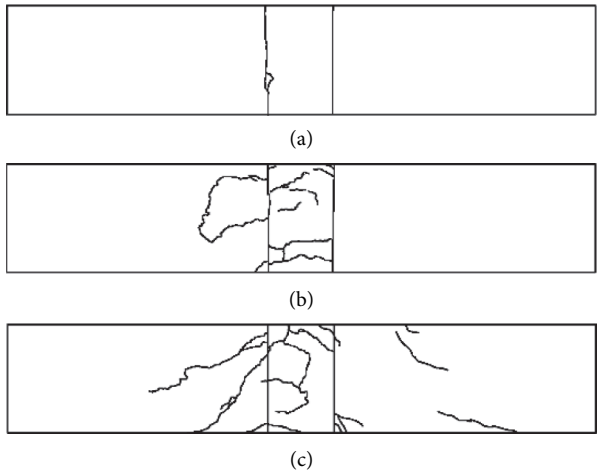

Figure 9: Crack pattern for specimens. (a) Type 1. (b) Type 2. (c) Type 3.

Figure 10: Failure modes for the specimens. (a) Type 1. (b) Type 2. (c) Type 3.

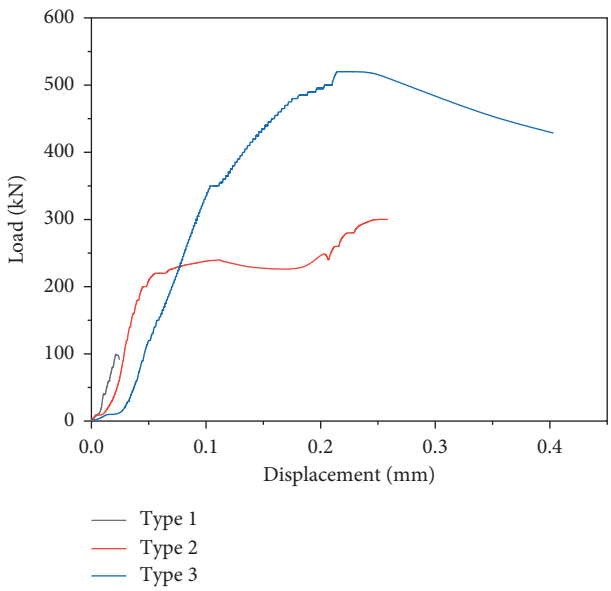

Figure 11: Load-displacement response.

Table 3: Ultimate shear strength of specimens (kN).

Specimen type	Ultimate shear strength	f_u/f_{u2} (%)
Type 1	99.6	33.1
Type 2	300.2	—
Type 3	520	173.2

Note. f_u is the ultimate shear strength of Type 1 and Type 3, and f_{u2} is the ultimate shear strength of Type 2.

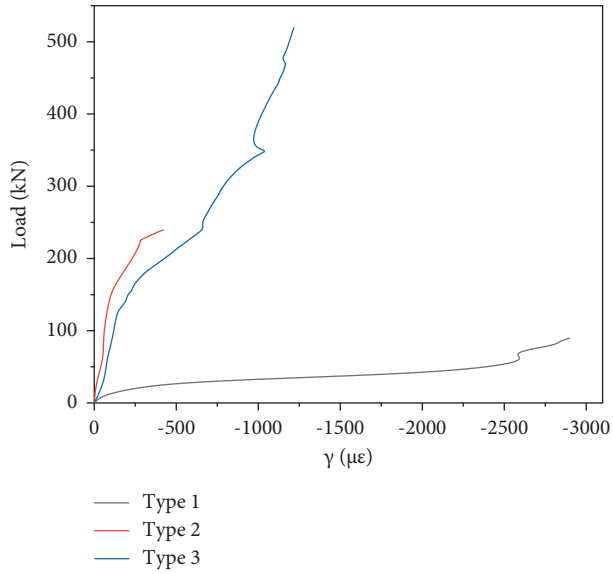

Figure 12: Load-shear strain curves of wet joints. *Note.* γ is the shear strain.

plasticity (CDP) constitutive model. This model is a continuum, plasticity-based, damage model for concrete; it is commonly used and adopted in ABAQUS. The CDP model defines that the two main failure mechanisms of the concrete are tensile cracking and compressive crushing. In this model, five variables or parameters are defined: ψ is the dilation angle, ε is the eccentricity, f_{b0}/f_{c0} is the ratio of initial biaxial compressive yield stress to initial uniaxial compressive yield stress, K is the ratio of the concrete strength under biaxial compression to the concrete strength under triaxial compression, and μ is the viscosity parameter. Table 4 shows the value of these variables or parameters. Table 4 shows the value of the parameters. Uniaxial compressive stress-strain curve, tension-strain curve, and damage evolution of concrete are selected from the code [28]. The constitutive model of the steel is a bilinear model. Poisson's ratio of concrete and steel is 0.2 and 0.3, respectively.

In order to analyze the stress and failure of the shear key, the model of concrete in this study adopts solid elements (C3D8R). Truss element (T3D2) is used for reinforcements. The mesh sizes of concrete of Type 1 and Type 3 are 25 mm × 25 mm. The mesh sizes of panels of Type 2 are 30 mm × 30 mm and the wet joint is 20 mm × 20 mm. The mesh of reinforcements is 25 mm. The interface of the panel and wet joint, boundary conditions, and loading conditions are shown in Figure 17. General contact is used for the interaction of the panels and wet joints. The contact with tangential, normal, and cohesive behavior is selected for the interaction property. The cohesive contact is used to simulate the interface of the concrete and concrete.

5.1. Crack Patterns. In order to show the crack growth of the specimen, the constitutive model "DAMAGET," assumed to be a plastic strain, is used to describe the tensile failure of concrete.

Figure 18(a) shows the crack distribution of Type 1 at failure. It can be seen from the figure that the failure of the specimen occurs on the upper part of the interaction of the wet joint and the bridge panel, and the predicted result is similar to the experimental result. Figure 18(b) shows one of the shear key cracks for the first time, and Figure 18(c) shows the crack distribution of the shear key when the specimen is damaged. When the load reaches 87 kN, the crack first appeared on the left and right sides of the shear key and gradually propagated. The failure of the shear key in the FE model is similar to that of the specimen in Figure 10(a). Thus, the crack patterns obtained from simulation and experiment have a good agreement. However, the crack development of the shear key cannot be easily observed in the experiment but can be clearly seen from numerical results.

Figure 19(a) shows the state of Type 2 when the interface debonds, corresponding to the load at 232 kN. It can be seen that the concrete-concrete interface has a tensile failure, and the bridge panels also have local damage. Figure 19(b) shows the complete failure of the specimen at a load of 270 kN. As can be seen from the figure, the concrete-concrete interface is seriously damaged, the cracks in the middle of the wet joint and the small cracks at the bottom of the wet joint can be observed, while the bridge panels are further damaged. Compared with Figure 10(b), the simulation results are in desirable agreement with the experimental results.

Figure 20(a) shows the state of Type 3 when the interface debonds, corresponding to the load at 310 kN. It can be seen from the figure that the concrete-concrete interface has a tensile failure. The concrete on the upper of bridge panels near the wet joint has a local tensile failure. Figure 20(b) shows the complete failure of the specimen with a load at 520 kN. At this time, the concrete-concrete interface debonds, and the concrete tensile failure occurs at the bottom of the wet joint and the middle of the two loading points. Figure 20(c) shows the state of the shear key when the interface debonds. The shear key is not damaged, but the concrete at the top of the bridge panel has tension damage. Figure 20(d) shows the state of the shear key when the specimen fails. At this time, the concrete at the bottom of the shear key is damaged, and the interface is almost debonding.

5.2. Ultimate Shear Capacity. The experiment mainly tests the ultimate shear capacity of the wet joint. In the experiment, a displacement sensor is set at the lower part of the wet joint. The load data of the experiment is provided by the servohydraulic testing machine, and the displacement data comes from the displacement sensor. In Figure 21(a), the finite element and experiment results of the ultimate shear

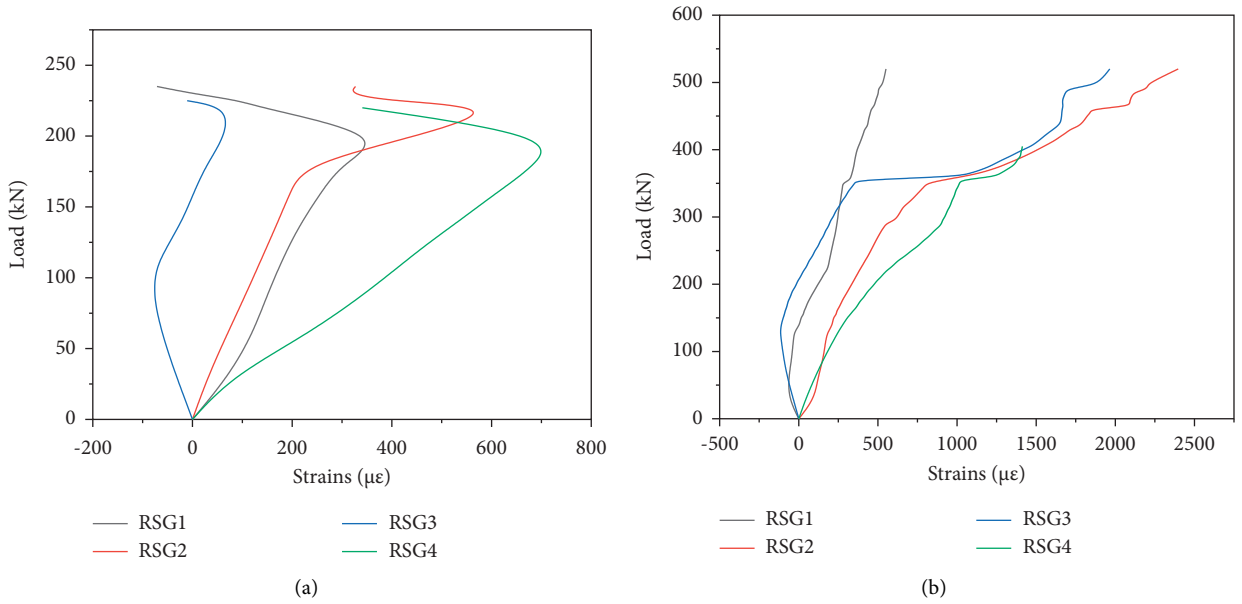

Figure 13: Load-strain curves of reinforcements. (a) Type 2. (b) Type 3.

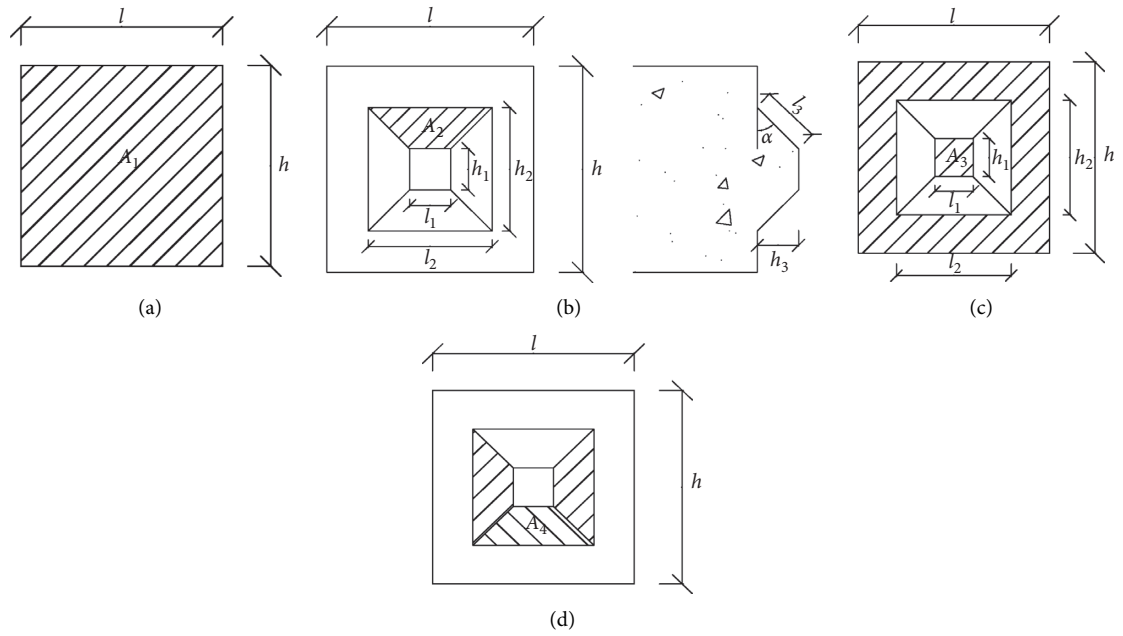

Figure 14: Detailed configurations of three specimens. (a) Configuration of Type 2. (b) Configuration of Type 1 and Type 3. (c) The area A_3. (d) The area A_4.

capacity of Type 1 are illustrated. The trend of numerical and experimental results shows good consistency. After reaching the ultimate shear capacity, the deformation of the wet joint decreases. The predicted values of ultimate shear force are very close to the measured values, about 100 kN, with an error of less than 1%.

In Figure 21(b), the finite element and experiment results of the ultimate shear capacity of Type 2 are illustrated. The slopes of these two result curves are close before yielding. The experimental and finite element results show that the slopes alter when the load reaches 220 kN and 232 kN. The reason for this variation of the slope of the curve is due to the existence of cracks in the concrete-concrete interface. These two result curves end after reaching the ultimate shear capacity of 300 kN and 270 kN. The load difference of interface failure between two results curves is 5%, while the ultimate shear capacity difference is 10%.

Figure 21(c) shows the ultimate shear capacity comparison of Type 2 between the finite element results and the experimental results. The slope of the curve between the

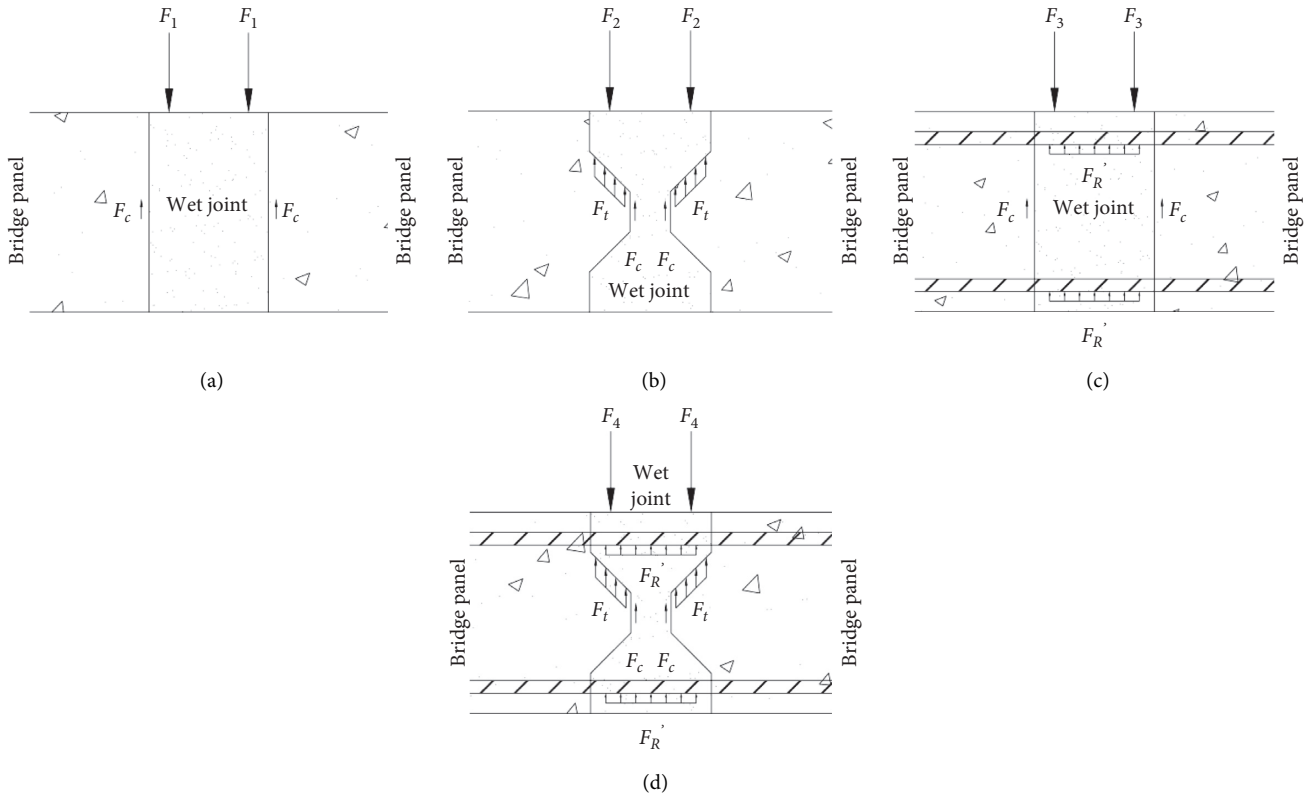

Figure 15: The load schemes of three specimens. (a) Wet joint with no shear key and reinforcement. (b) Loads on Type 1. (c) Loads on Type 2. (d) Loads on Type 3.

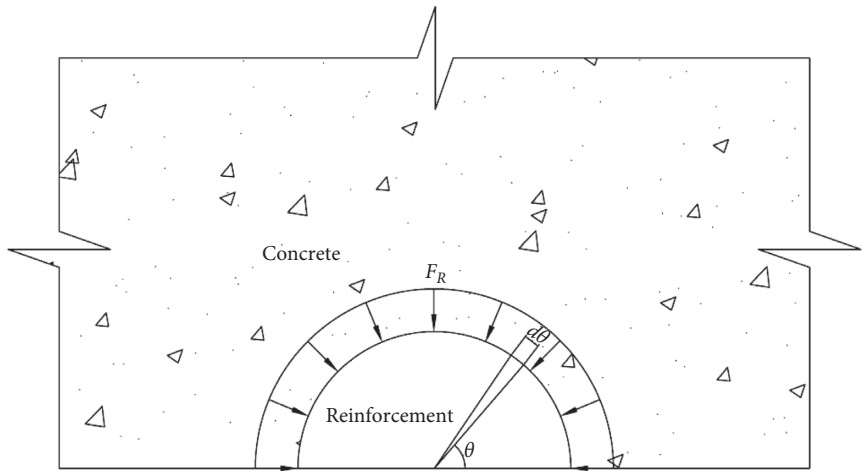

Figure 16: The force on reinforcement.

Table 4: Parameter of the concrete damage plasticity.

Parameter	ψ	ε	f_{b0}/f_{c0}	K	μ
Value	38°	0.1	1.16	0.67	0.001

experimental and the finite element results alters when the load reaches around 310 kN. The ultimate shear capacity of the experimental and finite element results is, respectively, 520 kN and 519 kN.

In Table 5, the experimental results, predicted results, and finite element results of the ultimate shear capacity of the specimens are compared. Both the theoretical and numerical results are in acceptable agreement with the experimental results.

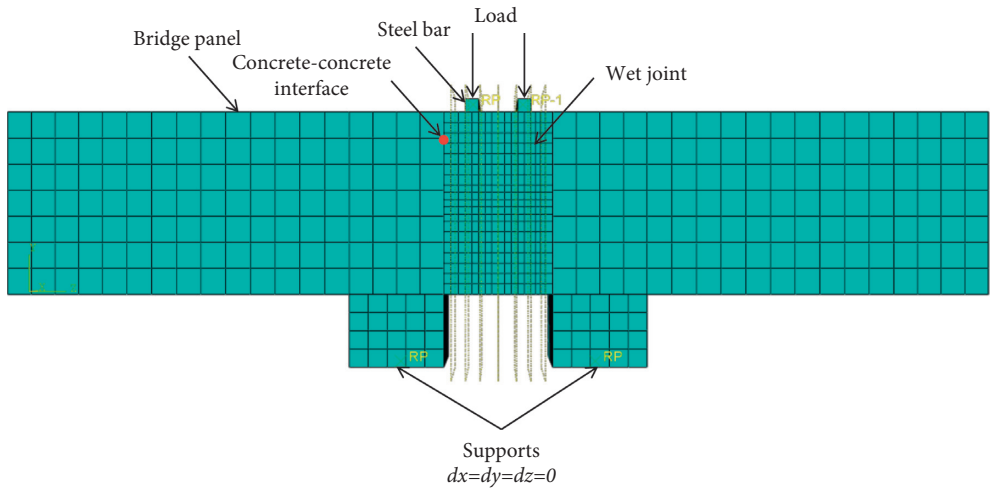

Figure 17: Mesh, boundary condition, and loading condition.

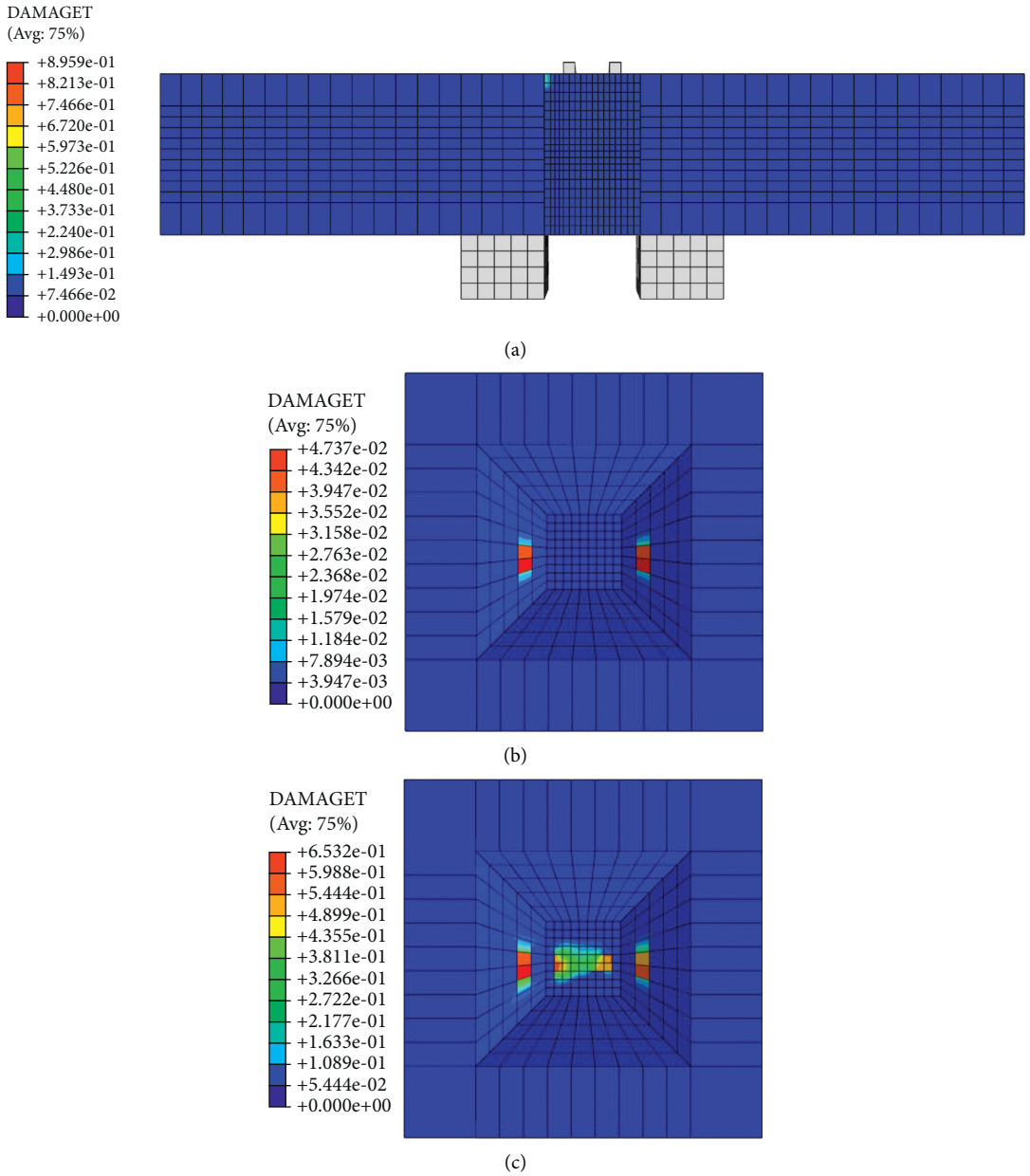

Figure 18: Crack patterns of Type 1. (a) Cracking patterns at failure. (b) Cracks at the first time. (c) Cracks at the failure of the shear key.

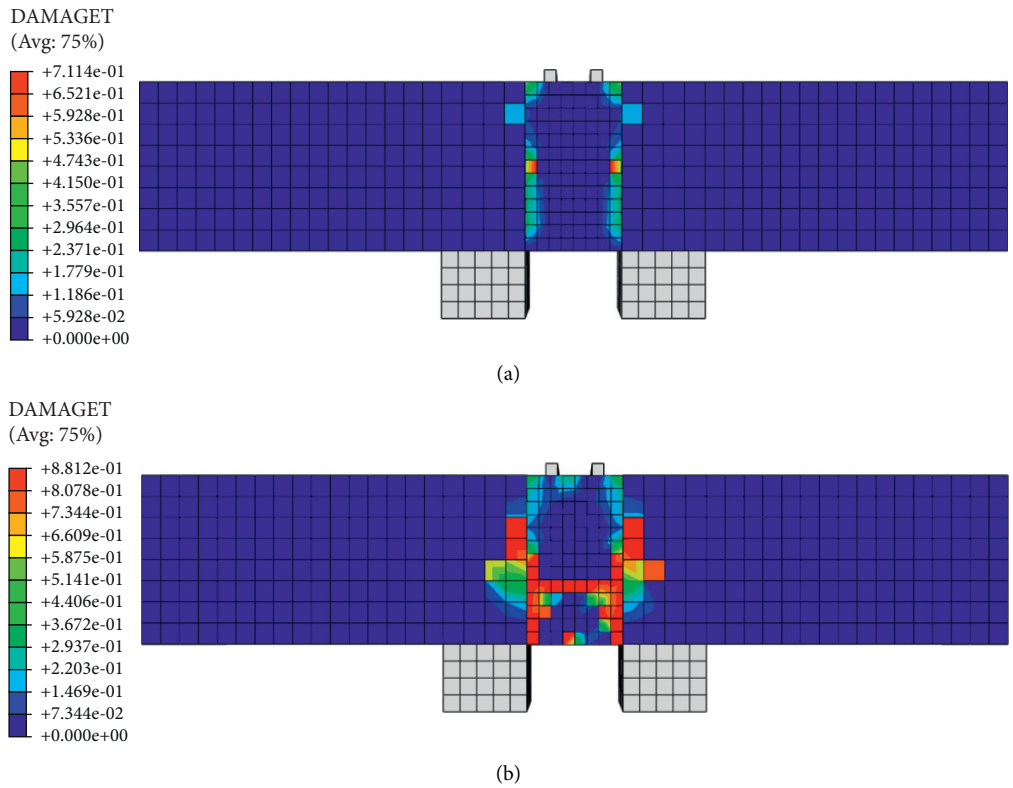

Figure 19: Cracking patterns of Type 2. (a) Initial interface cracking. (b) Cracking patterns at failure.

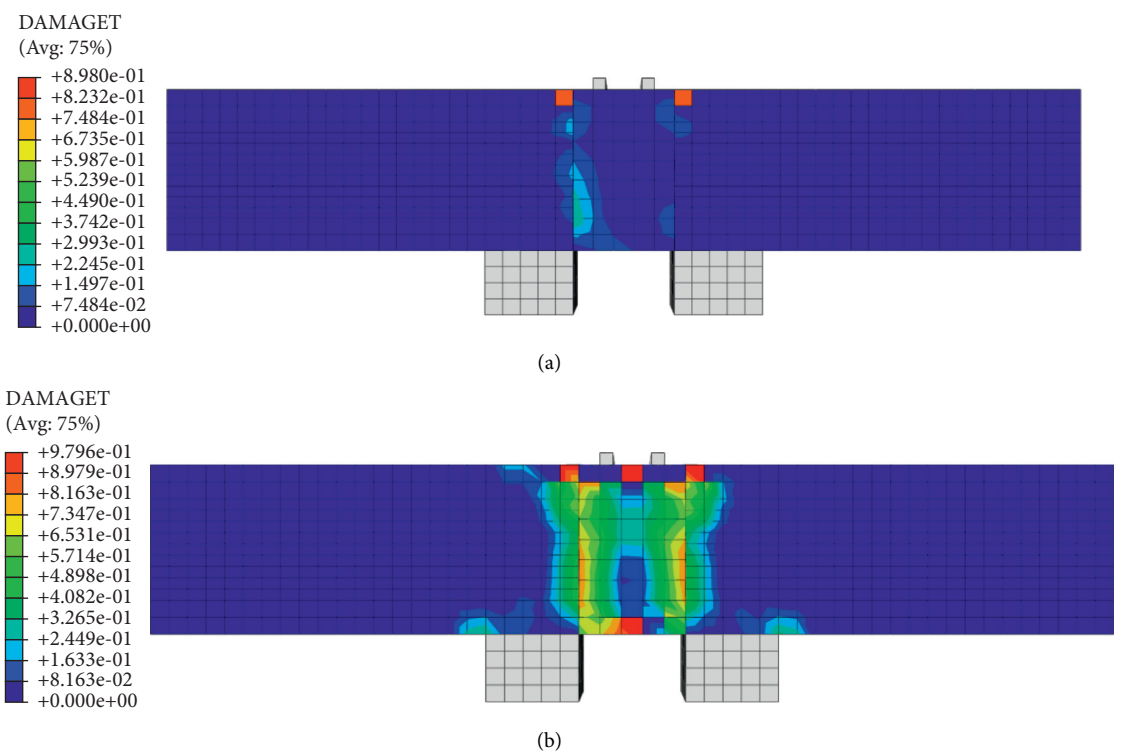

Figure 20: Continued.

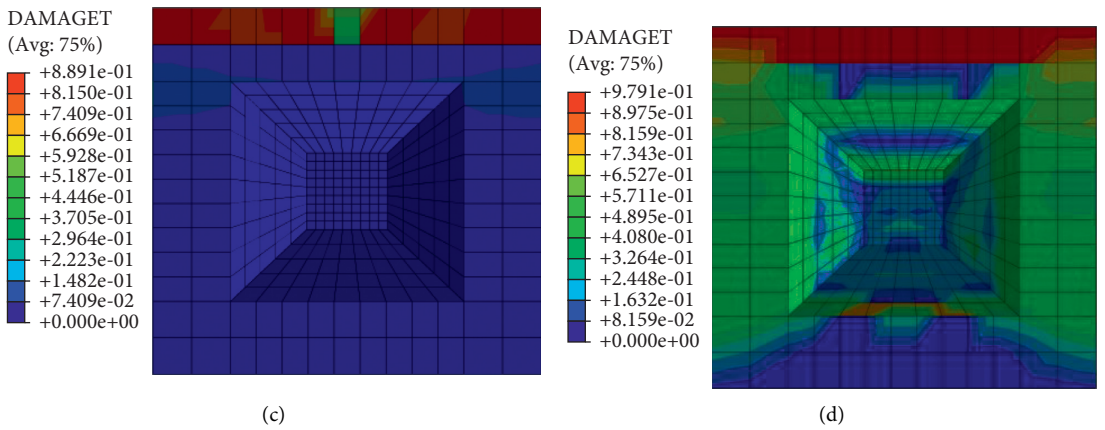

(c) (d)

Figure 20: Cracking patterns of Type 3. (a) Initial interface cracking. (b) Cracking patterns at failure. (c) State of the shear key at initial interface cracking. (d) State of the shear key in failure of the specimen.

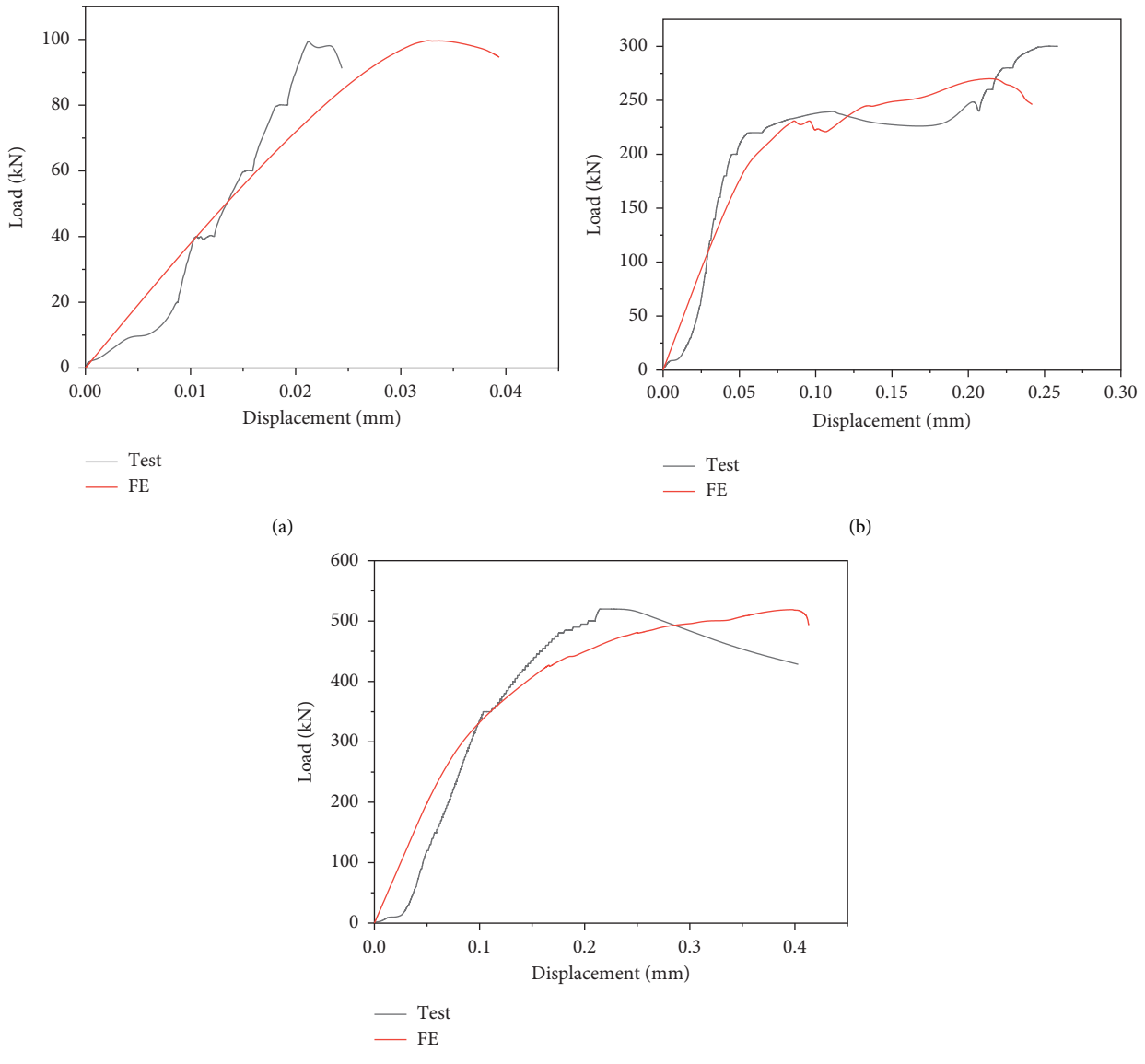

Figure 21: Load-displacement curves of experiment and finite element results. (a) Type 1. (b) Type 2. (c) Type 3.

Table 5: Comparison of experimental results, predicted results, and finite element results (unit: kN).

Specimens	Experimental result F_e	Predicted result F_t	$\lvert(F_t - F_e)/F_e\rvert$ (%)	Finite element result F_f	$\lvert F_f - F_e/F_e\rvert$ (%)
Type 1	99.6	96.0	3.6	99.6	0
Type 2	300.0	245.9	18.0	270.7	9.8
Type 3	520.0	415.9	20.0	519.3	0.1

6. Conclusions

A new type of concrete panel with a shear key is proposed, and specimens of this kind of bridge panel are fabricated. The shear capacity of the wet joint of the specimens is studied through experimental, theoretical, and numerical analysis. The mechanical properties of the specimens are discussed by analyzing ultimate shear stress, the displacement of the wet joint, the shear strain of the wet joint, and the strain of the reinforcement. The formulas of the shear strength are derived, and the finite element models of the specimens are considered for prediction. The main conclusions of this paper are as follows:

(1) In order to test the ultimate shear capacity of the wet joint, the experimental loading mode is designed. Through the experiment, under the same material characteristics, the ultimate shear capacity of the new wet joint structure is 73% higher than the conventional one

(2) Through numerical and experimental methods, the failure processes of three kinds of specimens are studied. The failure of Type 1 is illustrated, and the shear strain at the wet joint is very large. The failure of Type 2 is mainly caused by interfacial debonding. The interfacial debonding of Type 2 occurs from bottom to top along the concrete-concrete interface. The interfacial debonding of Type 3 occurs along the concrete-concrete interface. For Type 3, the shear key failure first occurs and then the interface debonds

(3) The formulas of the ultimate shear capacity of three specimens are derived, and the predicted results are in acceptable agreement with the experimental results

Data Availability

The data used to support the findings of this study are included within the article.

Conflicts of Interest

The authors declare that they have no conflicts of interest.

Acknowledgments

This research was substantially funded by the National Natural Science Foundation of China (No. 12072375).

References

[1] S. Saibabu, V. Srinivas, S. Sasmal, N. Lakshmanan, and N. R. Iyer, "Performance evaluation of dry and epoxy jointed segmental prestressed box girders under monotonic and cyclic loading," *Construction and Building Materials*, vol. 38, pp. 931–940, 2013.

[2] H. H. Hussein, K. K. Walsh, S. M. Sargand, and E. P. Steinberg, "Interfacial properties of ultrahigh-performance concrete and high-strength concrete bridge connections," *Journal of Materials in Civil Engineering*, vol. 5, no. 28, Article ID 4015208, 2016.

[3] B. Graybeal, *Design and Construction of Field-Cast UHPC Connections*, Federal highway administration, Washington, DC, USA, 2014.

[4] L. S. Verger, J. P. Charron, and B. Massicotte, "Design and behavior of UHPFRC field-cast transverse connections between precast bridge deck elements," *Journal of Bridge Engineering*, vol. 22, no. 7, Article ID 4017031, 2017.

[5] A. Arafa, A. S. Farghaly, E. A. Ahmed, and B. Benmokrane, "Laboratory testing of GFRP-RC panels with UHPFRC joints of the Nipigon River cable-stayed bridge in northwest Ontario, Canada," *Journal of Bridge Engineering*, vol. 21, no. 11, Article ID 5016006, 2016.

[6] M. H. Youssef, E. A. Ahmed, and B. Benmokrane, "Structural behavior of GFRP-RC bridge deck slabs connected with UHPFRC joints under flexure and shear," *Journal of Bridge Engineering*, vol. 24, no. 9, Article ID 4019092, 2019.

[7] J. Qi, Y. Bao, J. Wang, L. Li, and W. Li, "Flexural behavior of an innovative dovetail UHPC joint in composite bridges under negative bending moment," *Engineering Structures*, vol. 200, Article ID 109716, 2019.

[8] L. Li, Z. Ma, M. E. Griffey, and R. G. Oesterle, "Improved longitudinal joint details in decked bulb tees for accelerated bridge construction," *Concept development*, vol. 3, no. 15, pp. 327–336, 2009.

[9] L. Li, Z. Ma, and R. G. Oesterle, "Improved longitudinal joint details in decked bulb tees for accelerated bridge construction: fatigue evaluation," *Journal of Bridge Engineering*, vol. 5, no. 15, pp. 511–522, 2010.

[10] L. Li and Z. Jiang, "Flexural behavior and strut-and-tie model of joints with headed bar details connecting precast members," *Perspectives in Science*, vol. 7, pp. 253–260, 2016.

[11] S. Nasrin and A. Ibrahim, "Finite-element modeling of UHPC hybrid bridge deck connections," *International Journal of Advanced Structural Engineering*, vol. 10, no. 3, pp. 199–210, 2018.

[12] Z. B. Haber, "Lap-spliced rebar connections with UHPC closures," *Journal of Bridge Engineering*, vol. 23, no. 6, Article ID 4018028, 2018.

[13] W. H. Pan, J. S. Fan, J. G. Nie, J. H. Hu, and J. F. Cui, "Experimental study on tensile behavior of wet joints in a prefabricated composite deck system composed of

Orthotropic steel deck and ultrathin reactive-powder concrete layer," *Journal of Bridge Engineering*, vol. 21, no. 10, Article ID 4016064, 2016.

[14] X. M. Zhou, N. Mickleborough, and Z. J. Li, "Shear strength of joints in precast concrete segmental bridges," *ACI Structural Journal*, vol. 1, no. 102, pp. 3–11, 2005.

[15] M. A. Issa and H. A. Abdalla, "Structural behavior of single key joints in precast concrete segmental bridges," *Journal of Bridge Engineering*, vol. 3, no. 12, pp. 315–324, 2007.

[16] G. Li, D. Yang, and Y. Lei, "Combined shear and bending behavior of joints in precast concrete segmental beams with external tendons," *Journal of Bridge Engineering*, vol. 18, no. 10, pp. 1042–1052, 2013.

[17] Y. L. Voo, S. J. Foster, and C. C. Voo, "Ultrahigh-performance concrete segmental bridge technology: toward sustainable bridge construction," *Journal of Bridge Engineering*, vol. 20, no. 8, Article ID B5014001, 2015.

[18] H. Lee, J. Min, and W. Chung, "Full-scale testing of precast concrete bridge using internal connector in negative moment region," *Advances in Civil Engineering*, vol. 2019, no. 1, 12 pages, Article ID 6309859, 2019.

[19] H. H. Hussein, K. K. Walsh, S. M. Sargand, F. T. Al Rikabi, and E. P. Steinberg, "Modeling the shear connection in adjacent box-beam bridges with ultrahigh-performance concrete joints. I: model calibration and validation," *Journal of Bridge Engineering*, vol. 22, no. 8, Article ID 4017043, 2017.

[20] S. M. Sargand, K. K. Walsh, H. H. Hussein, F. T. Al Rikabi, and E. P. Steinberg, "Modeling the shear connection in adjacent box-beam bridges with ultrahigh-performance concrete joints. II: load transfer mechanism," *Journal of Bridge Engineering*, vol. 22, no. 8, Article ID 4017044, 2017.

[21] H. H. Hussein, S. M. Sargand, and I. Khoury, "Field investigation of ultra-high performance concrete shear key in an adjacent box-girder bridge," *Structure and Infrastructure Engineering*, vol. 15, no. 5, pp. 663–678, 2019.

[22] M. Noel, N. Wahab, and K. Soudki, "Experimental investigation of connection details for precast deck panels on concrete girders in composite deck construction," *Engineering Structures*, vol. 106, pp. 15–24, 2016.

[23] C. Zhao, K. Wang, Q. Zhou, K. Deng, and B. Cui, "Full-scale test and simulation on flexural behavior of dovetail-shaped reactive powder–concrete wet joint in a composite deck system," *Journal of Bridge Engineering*, vol. 8, no. 23, Article ID 4018051, 2018.

[24] P. M. D. Santos and E. N. B. S. Júlio, "A state-of-the-art review on shear-friction," *Engineering Structures*, vol. 45, pp. 435–448, 2012.

[25] P. M. D. Santos and E. N. B. S. Júlio, "A state-of-the-art review on roughness quantification methods for concrete surfaces," *Construction and Building Materials*, vol. 38, pp. 912–923, 2013.

[26] M. E. Mohamad, I. S. Ibrahim, R. Abdullah, A. B. Rahman, A. B. H. Kueh, and J. Usman, "Friction and cohesion coefficients of composite concrete-to-concrete bond," *Cement and Concrete Composites*, vol. 56, pp. 1–14, 2015.

[27] K. S. Rebeiz, "Shear strength prediction for concrete members," *Journal of Structural Engineering*, vol. 125, no. 3, pp. 301–308, 1999.

[28] Gb 50010-2010, *Code for Design of Concrete Structures*, China Building Industry Press, Beijing, China, 2010.